Supplemental Material for "Observation of a Near-Threshold Structure in the K^+ Recoil Mass Spectra in $e^+e^- \to K^+(D_s^- D^{*0} + D_s^{*-} D^0)$"

M. Ablikim[1], M. N. Achasov[10,c], P. Adlarson[67], S. Ahmed[15], M. Albrecht[4], R. Aliberti[28], A. Amoroso[66A,66C], Q. An[63,50], Anita[21], X. H. Bai[57], Y. Bai[49], O. Bakina[29], R. Baldini Ferroli[23A], I. Balossino[24A], Y. Ban[39,k], K. Begzsuren[26], N. Berger[28], M. Bertani[23A], D. Bettoni[24A], F. Bianchi[66A,66C], J Biernat[67], J. Bloms[60], A. Bortone[66A,66C], I. Boyko[29], R. A. Briere[5], H. Cai[68], X. Cai[1,50], A. Calcaterra[23A], G. F. Cao[1,55], N. Cao[1,55], S. A. Cetin[54B], J. F. Chang[1,50], W. L. Chang[1,55], G. Chelkov[29,b], D. Y. Chen[6], G. Chen[1], H. S. Chen[1,55], M. L. Chen[1,50], S. J. Chen[36], X. R. Chen[25], Y. B. Chen[1,50], Z. J Chen[20,l], W. S. Cheng[66C], G. Cibinetto[24A], F. Cossio[66C], X. F. Cui[37], H. L. Dai[1,50], X. C. Dai[1,55], A. Dbeyssi[15], R. B. de Boer[4], D. Dedovich[29], Z. Y. Deng[1], A. Denig[28], I. Denysenko[29], M. Destefanis[66A,66C], F. De Mori[66A,66C], Y. Ding[34], C. Dong[37], J. Dong[1,50], L. Y. Dong[1,55], M. Y. Dong[1,50,55], X. Dong[68], S. X. Du[71], J. Fang[1,50], S. S. Fang[1,55], Y. Fang[1], R. Farinelli[24A], L. Fava[66B,66C], F. Feldbauer[4], G. Felici[23A], C. Q. Feng[63,50], M. Fritsch[4], C. D. Fu[1], Y. Fu[1], Y. Gao[39,k], Y. Gao[64], Y. Gao[63,50], Y. G. Gao[6], I. Garzia[24A,24B], E. M. Gersabeck[58], A. Gilman[59], K. Goetzen[11], L. Gong[34], W. X. Gong[1,50], W. Gradl[28], M. Greco[66A,66C], L. M. Gu[36], M. H. Gu[1,50], S. Gu[2], Y. T. Gu[13], C. Y Guan[1,55], A. Q. Guo[22], L. B. Guo[35], R. P. Guo[41], Y. P. Guo[9,h], Y. P. Guo[28], A. Guskov[29], T. T. Han[42], X. Q. Hao[16], F. A. Harris[56], K. L. He[1,55], F. H. Heinsius[4], C. H. Heinz[28], T. Held[4], Y. K. Heng[1,50,55], C. Herold[52], M. Himmelreich[11,f], T. Holtmann[4], Y. R. Hou[55], Z. L. Hou[1], H. M. Hu[1,55], J. F. Hu[48,m], T. Hu[1,50,55], Y. Hu[1], G. S. Huang[63,50], L. Q. Huang[64], X. T. Huang[42], Y. P. Huang[1], Z. Huang[39,k], N. Huesken[60], T. Hussain[65], W. Ikegami Andersson[67], W. Imoehl[22], M. Irshad[63,50], S. Jaeger[4], S. Janchiv[26,j], Q. Ji[1], Q. P. Ji[16], X. B. Ji[1,55], X. L. Ji[1,50], H. B. Jiang[42], X. S. Jiang[1,50,55], X. Y. Jiang[37], Y. Jiang[55], J. B. Jiao[42], Z. Jiao[18], S. Jin[36], Y. Jin[57], T. Johansson[67], N. Kalantar-Nayestanaki[31], X. S. Kang[34], R. Kappert[31], M. Kavatsyuk[31], B. C. Ke[44,1], I. K. Keshk[4], A. Khoukaz[60], P. Kiese[28], R. Kiuchi[1], R. Kliemt[11], L. Koch[30], O. B. Kolcu[54B,e], B. Kopf[4], M. Kuemmel[4], M. Kuessner[4], A. Kupsc[67], M. G. Kurth[1,55], W. Kühn[30], J. J. Lane[58], J. S. Lange[30], P. Larin[15], L. Lavezzi[66A,66C], Z. H. Lei[63,50], H. Leithoff[28], M. Lellmann[28], T. Lenz[28], C. Li[40], C. H. Li[33], Cheng Li[63,50], D. M. Li[71], F. Li[1,50], G. Li[1], H. Li[44], H. Li[63,50], H. B. Li[1,55], H. J. Li[9,h], J. L. Li[42], J. Q. Li[4], Ke Li[1], L. K. Li[1], Lei Li[3], P. L. Li[63,50], P. R. Li[32,n,o], S. Y. Li[53], W. D. Li[1,55], W. G. Li[1], X. H. Li[63,50], X. L. Li[42], Z. Y. Li[51], H. Liang[63,50], H. Liang[1,55], Y. F. Liang[46], Y. T. Liang[25], L. Z. Liao[1,55], J. Libby[21], C. X. Lin[51], B. J. Liu[1], C. X. Liu[1], D. Liu[63,50], F. H. Liu[45], Fang Liu[1], Feng Liu[6], H. B. Liu[13], H. M. Liu[1,55], Huanhuan Liu[1], Huihui Liu[17], J. B. Liu[63,50], J. Y. Liu[1,55], K. Liu[1], K. Y. Liu[34], Ke Liu[6], L. Liu[63,50], M. H. Liu[9,h], Q. Liu[55], S. B. Liu[63,50], Shuai Liu[47], T. Liu[1,55], W. M. Liu[63,50], X. Liu[32], Y. Liu[32], Y. B. Liu[37], Z. A. Liu[1,50,55], Z. Q. Liu[42], X. C. Lou[1,50,55], F. X. Lu[16], H. J. Lu[18], J. D. Lu[1,55], J. G. Lu[1,50], X. L. Lu[1], Y. Lu[1], Y. P. Lu[1,50], C. L. Luo[35], M. X. Luo[70], P. W. Luo[51], T. Luo[9,h], X. L. Luo[1,50], S. Lusso[66C], X. R. Lyu[55], F. C. Ma[34], H. L. Ma[1], L. L. Ma[42], M. M. Ma[1,55], Q. M. Ma[1], R. Q. Ma[1,55], R. T. Ma[55], X. N. Ma[37], X. X. Ma[1,55], X. Y. Ma[1,50], F. E. Maas[15], M. Maggiora[66A,66C], S. Maldaner[28], S. Malde[61], Q. A. Malik[65], A. Mangoni[23B], Y. J. Mao[39,k], Z. P. Mao[1], S. Marcello[66A,66C], Z. X. Meng[57], J. G. Messchendorp[31], G. Mezzadri[24A], T. J. Min[36], R. E. Mitchell[22], X. H. Mo[1,50,55], Y. J. Mo[6], N. Yu. Muchnoi[10,c], H. Muramatsu[59], S. Nakhoul[11,f], Y. Nefedov[29], F. Nerling[11,f], I. B. Nikolaev[10,c], Z. Ning[1,50], S. Nisar[8,i], S. L. Olsen[55], Q. Ouyang[1,50,55], S. Pacetti[23B,23C], X. Pan[9,h], Y. Pan[58], A. Pathak[1], P. Patteri[23A], M. Pelizaeus[4], H. P. Peng[63,50], K. Peters[11,f], J. Pettersson[67], J. L. Ping[35], R. G. Ping[1,55], A. Pitka[4], R. Poling[59], V. Prasad[63,50], H. Qi[63,50], H. R. Qi[53], K. H. Qi[25], M. Qi[36], T. Y. Qi[9], T. Y. Qi[2], S. Qian[1,50], W. B. Qian[55], Z. Qian[51], C. F. Qiao[55], L. Q. Qin[12], X. S. Qin[42], Z. H. Qin[1,50], J. F. Qiu[1], S. Q. Qu[37], K. H. Rashid[65], K. Ravindran[21], C. F. Redmer[28], A. Rivetti[66C], V. Rodin[31], M. Rolo[66C], G. Rong[1,55], Ch. Rosner[15], M. Rump[60], H. S. Sang[63], A. Sarantsev[29,d], Y. Schelhaas[28], C. Schnier[4], K. Schoenning[67], M. Scodeggio[24A], D. C. Shan[47], W. Shan[19], X. Y. Shan[63,50], M. Shao[63,50], C. P. Shen[9], P. X. Shen[37], X. Y. Shen[1,55], B. A. Shi[55], H. C. Shi[63,50], R. S. Shi[1,55], X. Shi[1,50], X. D Shi[63,50], W. M. Song[27,1], Y. X. Song[39,k], S. Sosio[66A,66C], S. Spataro[66A,66C], K. X. Su[68], F. F. Sui[42], G. X. Sun[1], H. K. Sun[1], J. F. Sun[16], L. Sun[68], S. S. Sun[1,55], T. Sun[1,55], W. Y. Sun[35], X Sun[20,l], Y. J. Sun[63,50], Y. K. Sun[63,50], Y. Z. Sun[1], Z. T. Sun[1], Y. H. Tan[68], Y. X. Tan[63,50], C. J. Tang[46], G. Y. Tang[1], J. Tang[51], J. X. Teng[63,50], V. Thoren[67], I. Uman[54D], C. W. Wang[36], D. Y. Wang[39,k], H. J. Wang[55], H. P. Wang[1,55], K. Wang[1,50], L. L. Wang[1], M. Wang[42], M. Z. Wang[39,k], Meng Wang[1,55], W. H. Wang[68], W. P. Wang[63,50], X. Wang[39,k], X. F. Wang[32], X. L. Wang[9,h], Y. Wang[51], Y. Wang[63,50], Y. D. Wang[38], Y. F. Wang[1,50,55], Y. Q. Wang[1], Z. Wang[1,50], Z. Y. Wang[1], Ziyi Wang[55], Zongyuan Wang[1,55], D. H. Wei[12], P. Weidenkaff[28], F. Weidner[60], S. P. Wen[1], D. J. White[58], U. Wiedner[4], G. Wilkinson[61], M. Wolke[67], L. Wollenberg[4], J. F. Wu[1,55], L. H. Wu[1], L. J. Wu[1,55], X. Wu[9,h], Z. Wu[1,50], L. Xia[63,50], H. Xiao[9,h], S. Y. Xiao[1], Y. J. Xiao[1,55], Z. J. Xiao[35], X. H. Xie[39,k], Y. G. Xie[1,50], Y. H. Xie[6], T. Y. Xing[1,55], G. F. Xu[1], J. J. Xu[36], Q. J. Xu[14], W. Xu[1,55], X. P. Xu[47], Y. C. Xu[55], F. Yan[9,h], L. Yan[66A,66C], L. Yan[9,h], W. B. Yan[63,50], W. C. Yan[71], Xu Yan[47], H. J. Yang[43,g], H. X. Yang[1], L. Yang[44], R. X. Yang[63,50], S. L. Yang[55], S. L. Yang[1,55], Y. H. Yang[36], Y. X. Yang[12], Yifan Yang[1,55], Zhi Yang[25], M. Ye[1,50], M. H. Ye[7], J. H. Yin[1], Z. Y. You[51], B. X. Yu[1,50,55], C. X. Yu[37], G. Yu[1,55], J. S. Yu[20,l], T. Yu[64], C. Z. Yuan[1,55], L. Yuan[2], W. Yuan[66A,66C], X. Q. Yuan[39,k], Y. Yuan[1], Z. Y. Yuan[51], C. X. Yue[33], A. Yuncu[54B,a], A. A. Zafar[65], Y. Zeng[20,l], B. X. Zhang[1], Guangyi Zhang[16], H. Zhang[63], H. H. Zhang[51], H. Y. Zhang[1,50], J. J. Zhang[44], J. L. Zhang[69], J. Q. Zhang[4], J. W. Zhang[1,50,55], J. Y. Zhang[1], J. Z. Zhang[1,55], Jianyu Zhang[1,55], Jiawei Zhang[1,55], Lei Zhang[36], S. Zhang[51], S. F. Zhang[36], Shulei Zhang[20,l], X. D. Zhang[38], X. Y. Zhang[42], Y. Zhang[61], Y. H. Zhang[1,50], Y. T. Zhang[63,50], Yan Zhang[63,50], Yao Zhang[1], Yi Zhang[9,h], Z. H. Zhang[6], Z. Y. Zhang[68], G. Zhao[1], J. Zhao[33], J. Y. Zhao[1,55], J. Z. Zhao[1,50], Lei Zhao[63,50], Ling Zhao[1], M. G. Zhao[37], Q. Zhao[1], S. J. Zhao[71], Y. B. Zhao[1,50], Y. X. Zhao[25], Z. G. Zhao[63,50], A. Zhemchugov[29,b], B. Zheng[64], J. P. Zheng[1,50], Y. Zheng[39,k], Y. H. Zheng[55], B. Zhong[35], C. Zhong[64], L. P. Zhou[1,55], Q. Zhou[1,55], X. Zhou[68], X. K. Zhou[55], X. R. Zhou[63,50], A. N. Zhu[1,55], J. Zhu[37], K. Zhu[1], K. J. Zhu[1,50,55], S. H. Zhu[62], T. J. Zhu[69], W. J. Zhu[37], X. L. Zhu[53], Y. C. Zhu[63,50], Z. A. Zhu[1,55], B. S. Zou[1], J. H. Zou[1]

(BESIII Collaboration)

[1] *Institute of High Energy Physics, Beijing 100049, People's Republic of China*
[2] *Beihang University, Beijing 100191, People's Republic of China*
[3] *Beijing Institute of Petrochemical Technology, Beijing 102617, People's Republic of China*
[4] *Bochum Ruhr-University, D-44780 Bochum, Germany*
[5] *Carnegie Mellon University, Pittsburgh, Pennsylvania 15213, USA*
[6] *Central China Normal University, Wuhan 430079, People's Republic of China*
[7] *China Center of Advanced Science and Technology, Beijing 100190, People's Republic of China*
[8] *COMSATS University Islamabad, Lahore Campus, Defence Road, Off Raiwind Road, 54000 Lahore, Pakistan*
[9] *Fudan University, Shanghai 200443, People's Republic of China*
[10] *G.I. Budker Institute of Nuclear Physics SB RAS (BINP), Novosibirsk 630090, Russia*
[11] *GSI Helmholtzcentre for Heavy Ion Research GmbH, D-64291 Darmstadt, Germany*
[12] *Guangxi Normal University, Guilin 541004, People's Republic of China*
[13] *Guangxi University, Nanning 530004, People's Republic of China*
[14] *Hangzhou Normal University, Hangzhou 310036, People's Republic of China*
[15] *Helmholtz Institute Mainz, Johann-Joachim-Becher-Weg 45, D-55099 Mainz, Germany*
[16] *Henan Normal University, Xinxiang 453007, People's Republic of China*
[17] *Henan University of Science and Technology, Luoyang 471003, People's Republic of China*
[18] *Huangshan College, Huangshan 245000, People's Republic of China*
[19] *Hunan Normal University, Changsha 410081, People's Republic of China*
[20] *Hunan University, Changsha 410082, People's Republic of China*
[21] *Indian Institute of Technology Madras, Chennai 600036, India*
[22] *Indiana University, Bloomington, Indiana 47405, USA*
[23] *INFN Laboratori Nazionali di Frascati , (A)INFN Laboratori Nazionali di Frascati, I-00044, Frascati, Italy; (B)INFN Sezione di Perugia, I-06100, Perugia, Italy*
[24] *INFN Sezione di Ferrara, INFN Sezione di Ferrara, I-44122, Ferrara, Italy*
[25] *Institute of Modern Physics, Lanzhou 730000, People's Republic of China*
[26] *Institute of Physics and Technology, Peace Ave. 54B, Ulaanbaatar 13330, Mongolia*
[27] *Jilin University, Changchun 130012, People's Republic of China*
[28] *Johannes Gutenberg University of Mainz, Johann-Joachim-Becher-Weg 45, D-55099 Mainz, Germany*
[29] *Joint Institute for Nuclear Research, 141980 Dubna, Moscow region, Russia*
[30] *Justus-Liebig-Universitaet Giessen, II. Physikalisches Institut, Heinrich-Buff-Ring 16, D-35392 Giessen, Germany*
[31] *KVI-CART, University of Groningen, NL-9747 AA Groningen, The Netherlands*
[32] *Lanzhou University, Lanzhou 730000, People's Republic of China*
[33] *Liaoning Normal University, Dalian 116029, People's Republic of China*
[34] *Liaoning University, Shenyang 110036, People's Republic of China*
[35] *Nanjing Normal University, Nanjing 210023, People's Republic of China*
[36] *Nanjing University, Nanjing 210093, People's Republic of China*
[37] *Nankai University, Tianjin 300071, People's Republic of China*
[38] *North China Electric Power University, Beijing 102206, People's Republic of China*
[39] *Peking University, Beijing 100871, People's Republic of China*
[40] *Qufu Normal University, Qufu 273165, People's Republic of China*
[41] *Shandong Normal University, Jinan 250014, People's Republic of China*
[42] *Shandong University, Jinan 250100, People's Republic of China*
[43] *Shanghai Jiao Tong University, Shanghai 200240, People's Republic of China*
[44] *Shanxi Normal University, Linfen 041004, People's Republic of China*
[45] *Shanxi University, Taiyuan 030006, People's Republic of China*
[46] *Sichuan University, Chengdu 610064, People's Republic of China*
[47] *Soochow University, Suzhou 215006, People's Republic of China*
[48] *South China Normal University, Guangzhou 510006, People's Republic of China*
[49] *Southeast University, Nanjing 211100, People's Republic of China*
[50] *State Key Laboratory of Particle Detection and Electronics, Beijing 100049, Hefei 230026, People's Republic of China*
[51] *Sun Yat-Sen University, Guangzhou 510275, People's Republic of China*
[52] *Suranaree University of Technology, University Avenue 111, Nakhon Ratchasima 30000, Thailand*
[53] *Tsinghua University, Beijing 100084, People's Republic of China*
[54] *Turkish Accelerator Center Particle Factory Group, (A)Istanbul Bilgi University, 34060 Eyup, Istanbul, Turkey; (B)Near East University, Nicosia, North Cyprus, Mersin 10, Turkey*
[55] *University of Chinese Academy of Sciences, Beijing 100049, People's Republic of China*
[56] *University of Hawaii, Honolulu, Hawaii 96822, USA*
[57] *University of Jinan, Jinan 250022, People's Republic of China*
[58] *University of Manchester, Oxford Road, Manchester, M13 9PL, United Kingdom*
[59] *University of Minnesota, Minneapolis, Minnesota 55455, USA*
[60] *University of Muenster, Wilhelm-Klemm-Str. 9, 48149 Muenster, Germany*

[61] University of Oxford, Keble Rd, Oxford, UK OX13RH
[62] University of Science and Technology Liaoning, Anshan 114051, People's Republic of China
[63] University of Science and Technology of China, Hefei 230026, People's Republic of China
[64] University of South China, Hengyang 421001, People's Republic of China
[65] University of the Punjab, Lahore-54590, Pakistan
[66] University of Turin and INFN, INFN, I-10125, Turin, Italy
[67] Uppsala University, Box 516, SE-75120 Uppsala, Sweden
[68] Wuhan University, Wuhan 430072, People's Republic of China
[69] Xinyang Normal University, Xinyang 464000, People's Republic of China
[70] Zhejiang University, Hangzhou 310027, People's Republic of China
[71] Zhengzhou University, Zhengzhou 450001, People's Republic of China

[a] Also at Bogazici University, 34342 Istanbul, Turkey
[b] Also at the Moscow Institute of Physics and Technology, Moscow 141700, Russia
[c] Also at the Novosibirsk State University, Novosibirsk, 630090, Russia
[d] Also at the NRC "Kurchatov Institute", PNPI, 188300, Gatchina, Russia
[e] Also at Istanbul Arel University, 34295 Istanbul, Turkey
[f] Also at Goethe University Frankfurt, 60323 Frankfurt am Main, Germany
[g] Also at Key Laboratory for Particle Physics, Astrophysics and Cosmology, Ministry of Education; Shanghai Key Laboratory for Particle Physics and Cosmology; Institute of Nuclear and Particle Physics, Shanghai 200240, People's Republic of China
[h] Also at Key Laboratory of Nuclear Physics and Ion-beam Application (MOE) and Institute of Modern Physics, Fudan University, Shanghai 200443, People's Republic of China
[i] Also at Harvard University, Department of Physics, Cambridge, MA, 02138, USA
[j] Currently at: Institute of Physics and Technology, Peace Ave.54B, Ulaanbaatar 13330, Mongolia
[k] Also at State Key Laboratory of Nuclear Physics and Technology, Peking University, Beijing 100871, People's Republic of China
[l] School of Physics and Electronics, Hunan University, Changsha 410082, China
[m] Also at Guangdong Provincial Key Laboratory of Nuclear Science, Institute of Quantum Matter, South China Normal University, Guangzhou 510006, China
[n] Frontiers Science Center for Rare Isotopes, Lanzhou University, Lanzhou 730000, People's Republic of China
[o] Lanzhou Center for Theoretical Physics, Lanzhou University, Lanzhou 730000, People's Republic of China

(Dated: **February 18, 2021)**

I. ADDITIONAL INFORMATION: STUDIES OF THE EXCESS IN K^+ RECOIL-MASS SPECTRUM

Figure 1 shows the distribution of the $K^+D_s^-$ recoil-mass in data and MC simulation samples at $\sqrt{s} = 4.628$, 4.641, 4.661 and 4.698 GeV, after the same selection criteria as those imposed for the data shown in Fig. 2 of the main letter. Table I lists the estimated sizes of excited D_s^{**+} or $\bar{D}^{**0}$ contributions at each energy point, quoted in the simultaneous fit. In addition, two-dimensional plots of $M(K^+D_s^-)$ versus $RM(K^+)$ in data for events in the signal region and WS events at $\sqrt{s} = 4.681$ GeV are shown in Fig. 2.

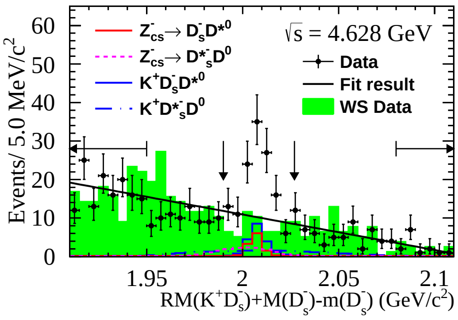

(a)Recoil mass of $K^+D_s^-$ at $\sqrt{s} = 4.628$ GeV.

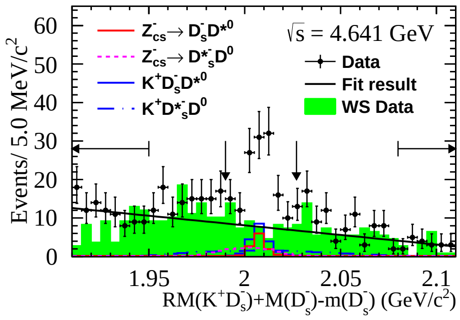

(b)Recoil mass of $K^+D_s^-$ at $\sqrt{s} = 4.641$ GeV.

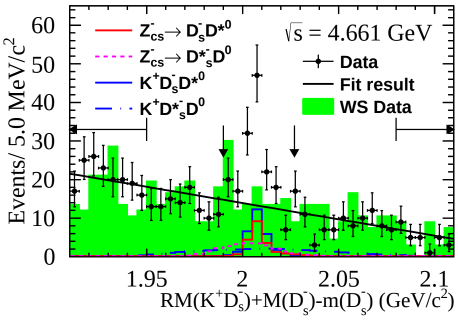

(c)Recoil mass of $K^+D_s^-$ at $\sqrt{s} = 4.661$ GeV.

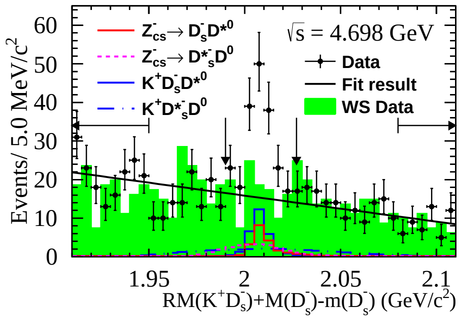

(d)Recoil mass of $K^+D_s^-$ at $\sqrt{s} = 4.698$ GeV.

FIG. 1. Distribution of the $K^+D_s^-$ recoil-mass in data and signal MC samples at different center-of-mass energies. Definitions of plotted components are the same as those in Fig. 2 of the main paper.

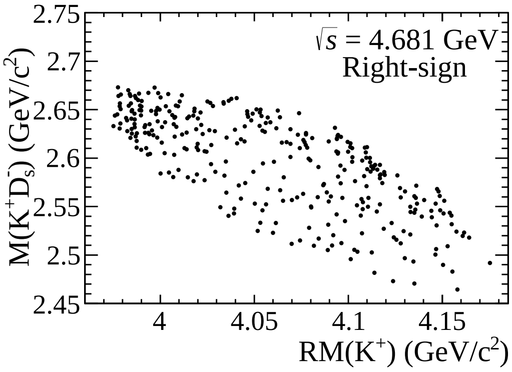

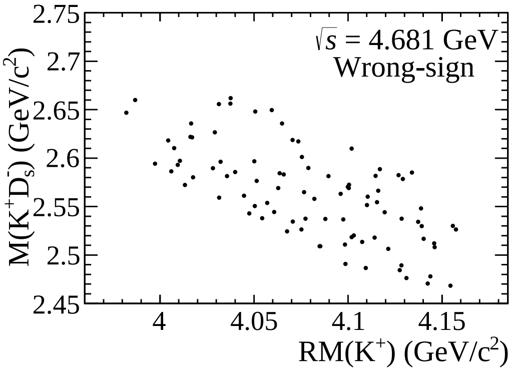

FIG. 2. Two-dimensional distributions of $M(K^+D_s^-)$ vs. $RM(K^+)$ for data in the signal region (left) and WS events (right) at $\sqrt{s} = 4.681$ GeV.

TABLE I. Summary of the estimated sizes of excited D_s^{**+} or $\bar{D}^{**0}$ contributions at each energy point. "–" means the production is not allowed kinematically.

$\sqrt{s}$(GeV)	4.628	4.641	4.661	4.681	4.698
$D_{s1}(2536)^+(K^+D^{*0})D_s^-$	41.2 ± 6.3	26.2 ± 5.4	23.9 ± 5.6	54.4 ± 8.0	15.3 ± 4.2
$D_{s2}^*(2573)^+(K^+D^0)D_s^{*-}$	–	–	–	19.1 ± 7.6	17.3 ± 7.3
$D_{s1}^*(2700)^+(K^+D^{*0})D_s^-$	0.0 ± 1.8	18.6 ± 8.7	16.6 ± 7.8	15.0 ± 13.3	7.7 ± 8.4
$\bar{D}_3^*(2750)^0(\to D_s^{*-}K^+)D^0$	0.0 ± 0.1	0.0 ± 0.2	0.0 ± 0.2	0.0 ± 0.4	0.0 ± 0.5

II. EXPLORATION OF POTENTIAL $D^{**}_{(s)}$ BACKGROUNDS

To understand the potential backgrounds from excited $D^{**}_{(s)}$ states, all reported states in the PDG [1] whose production and decay is allowed within the available phase-space at $\sqrt{s} = 4.681$ GeV are investigated. The corresponding $RM(K^+)$ distributions of the MC simulations are plotted in Figs. 3 and 4. Furthermore, possible interferences among those excited $D^{**}_{(s)}$ states are systematically scanned, and the choices with the largest interferences around $RM(K^+) = 4.0\,\mathrm{GeV}/c^2$ are compared with the distributions in data, shown in Fig. 5 and Fig. 6. It is evident that none of the states can explain the narrow peaking structure below $4.0\,\mathrm{GeV}/c^2$.

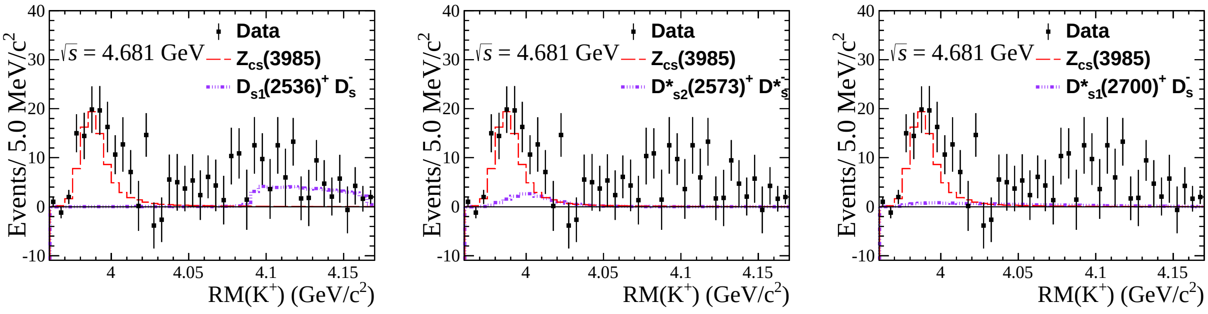

(a) $D_{s1}(2536)^+(\to D^{*0}K^+)D_s^-$ (b) $D^*_{s2}(2573)^+(\to D^0K^+)D_s^{*-}$ (c) $D^*_{s1}(2700)^+(\to D^{*0}K^+)D_s^-$

FIG. 3. K^+ recoil-mass spectra in data with the WS background contributions subtracted, and MC simulations of the excited D_s^{**} states in $e^+e^- \to D_s^{**+}D_s^{(*)-}$. The $Z_{cs}(3985)^-$ shapes are normalized to the yields observed in data and those of the D_s^{**} states are scaled according to the control samples.

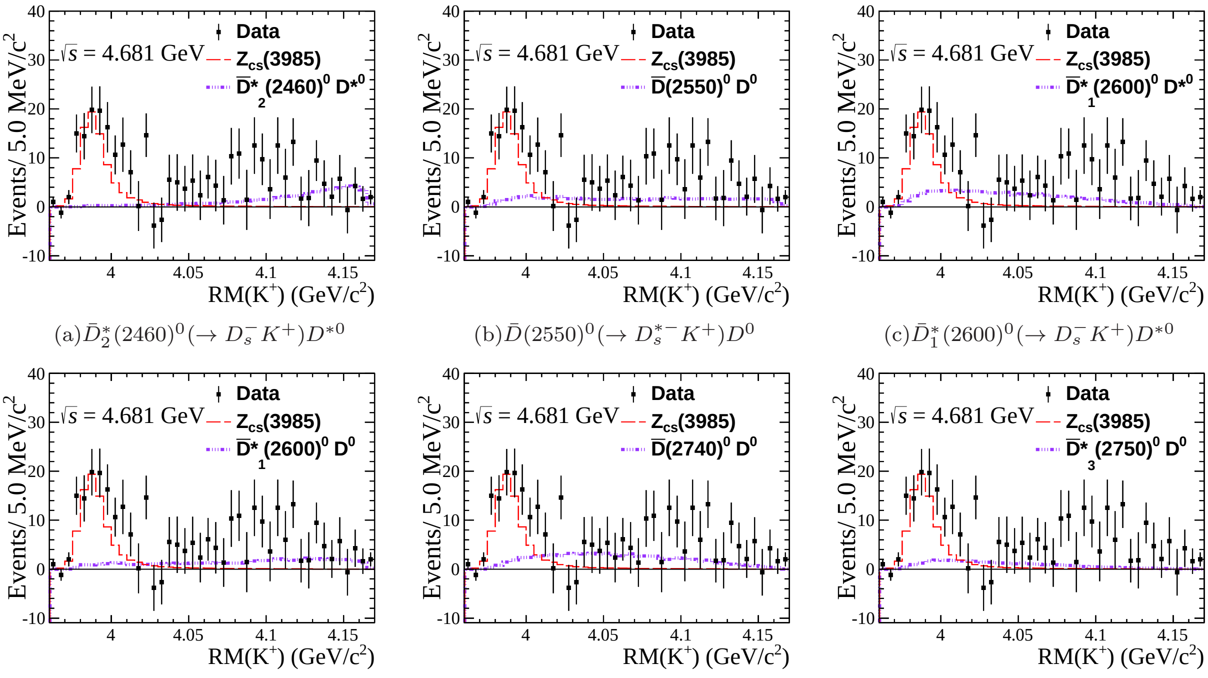

(a) $\bar{D}^*_2(2460)^0(\to D_s^-K^+)D^{*0}$ (b) $\bar{D}(2550)^0(\to D_s^{*-}K^+)D^0$ (c) $\bar{D}^*_1(2600)^0(\to D_s^-K^+)D^{*0}$

(d) $\bar{D}^*_1(2600)^0(\to D_s^{*-}K^+)D^0$ (e) $\bar{D}(2740)^0(\to D_s^{*-}K^+)D^0$ (f) $\bar{D}^*_3(2750)^0(\to D_s^{*-}K^+)D^0$

FIG. 4. K^+ recoil-mass spectra in data with the WS background contributions subtracted, and MC simulations of the excited D^{**} states in $e^+e^- \to \bar{D}^{**0}D^{(*)0}$. The $Z_{cs}(3985)^-$ shape is normalized to the yields observed in data and the shape of the $\bar{D}^{**0}$ states is arbitrarily scaled.

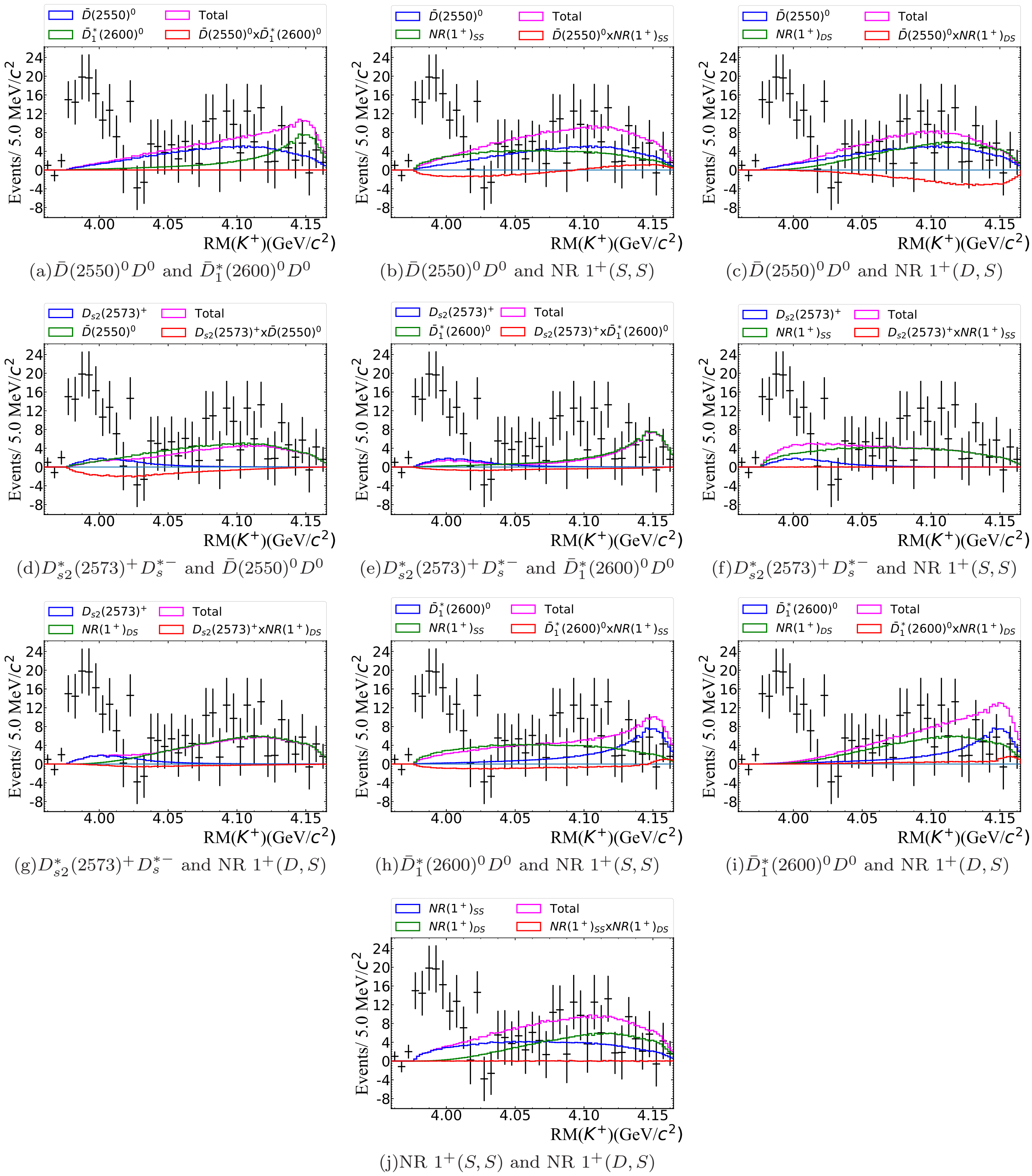

(a) $\bar{D}(2550)^0 D^0$ and $\bar{D}_1^*(2600)^0 D^0$

(b) $\bar{D}(2550)^0 D^0$ and NR $1^+(S,S)$

(c) $\bar{D}(2550)^0 D^0$ and NR $1^+(D,S)$

(d) $D_{s2}^*(2573)^+ D_s^{*-}$ and $\bar{D}(2550)^0 D^0$

(e) $D_{s2}^*(2573)^+ D_s^{*-}$ and $\bar{D}_1^*(2600)^0 D^0$

(f) $D_{s2}^*(2573)^+ D_s^{*-}$ and NR $1^+(S,S)$

(g) $D_{s2}^*(2573)^+ D_s^{*-}$ and NR $1^+(D,S)$

(h) $\bar{D}_1^*(2600)^0 D^0$ and NR $1^+(S,S)$

(i) $\bar{D}_1^*(2600)^0 D^0$ and NR $1^+(D,S)$

(j) NR $1^+(S,S)$ and NR $1^+(D,S)$

FIG. 5. K^+ recoil-mass spectra in data with the WS background contributions subtracted, and MC simulations of two possible background processes for the $K^+D_s^{*-}D^0$ final state, whose interferences are taken into account. The interference effect is tuned to be largest around $4.0\,\mathrm{GeV}/c^2$. In the non-resonant (NR) process, the angular momentum $(L_{K^+X}, L_{D_s^{*-}D^0})$ denotes the angular momentum between K^+ and $X_{D_s^{*-}D^0}$, and D_s^{*-} and D^0 in the $e^+e^-(X_{D_s^{*-}D^0})$ rest frame, respectively. Individual contributions are scaled according to the observed yields in the control samples.

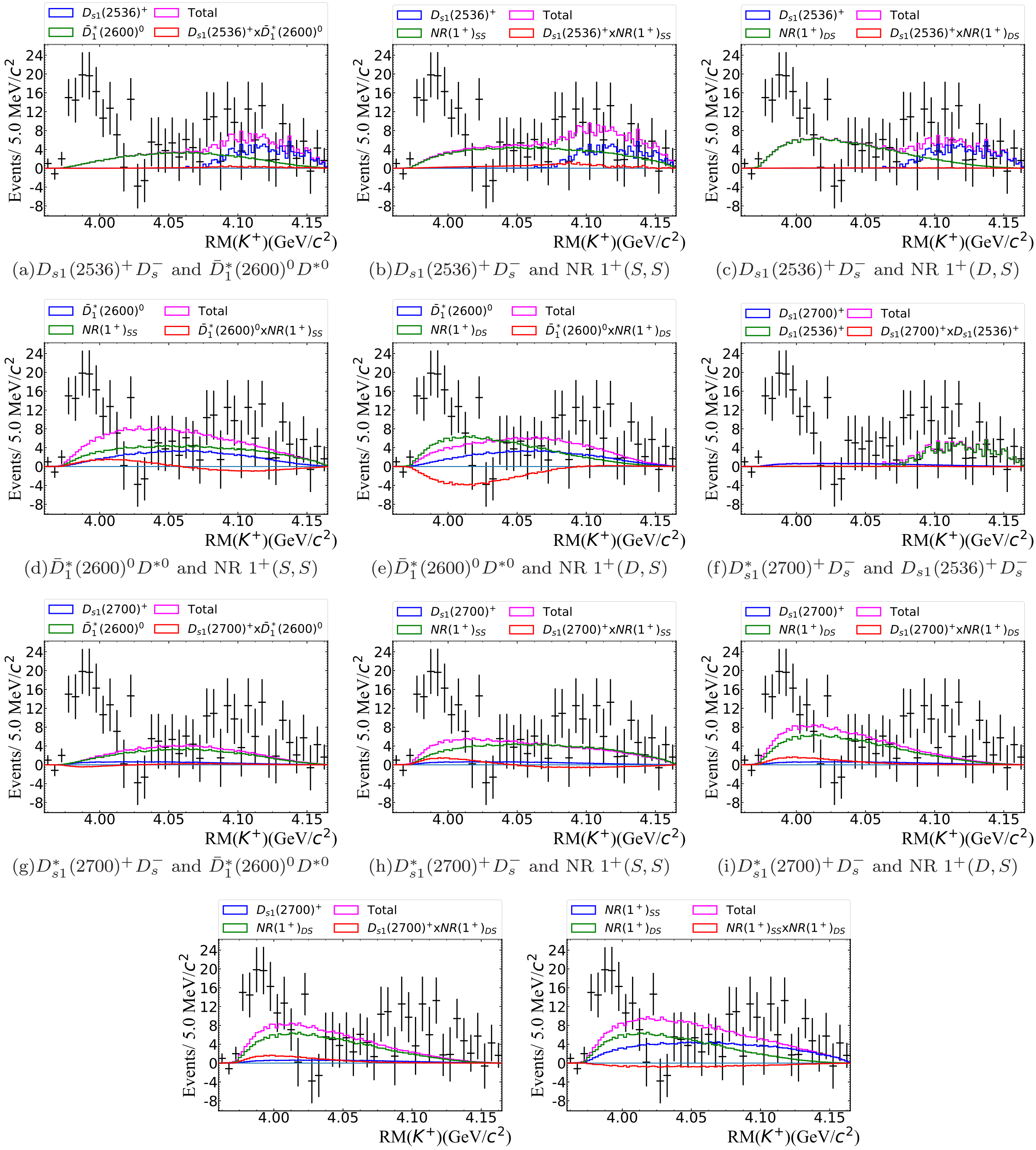

(a)$D_{s1}(2536)^+D_s^-$ and $\bar{D}_1^*(2600)^0D^{*0}$ (b)$D_{s1}(2536)^+D_s^-$ and NR $1^+(S,S)$ (c)$D_{s1}(2536)^+D_s^-$ and NR $1^+(D,S)$

(d)$\bar{D}_1^*(2600)^0D^{*0}$ and NR $1^+(S,S)$ (e)$\bar{D}_1^*(2600)^0D^{*0}$ and NR $1^+(D,S)$ (f)$D_{s1}^*(2700)^+D_s^-$ and $D_{s1}(2536)^+D_s^-$

(g)$D_{s1}^*(2700)^+D_s^-$ and $\bar{D}_1^*(2600)^0D^{*0}$ (h)$D_{s1}^*(2700)^+D_s^-$ and NR $1^+(S,S)$ (i)$D_{s1}^*(2700)^+D_s^-$ and NR $1^+(D,S)$

(j)$D_{s1}^*(2700)^+D_s^-$ and NR $1^+(D,S)$ (k)NR $1^+(S,S)$ and NR $1^+(D,S)$

FIG. 6. K^+ recoil-mass spectra in data with the WS background contributions subtracted, and MC simulations of two possible background processes for the $K^+D_s^-D^{*0}$ final state, whose interferences are taken into account. The interference effect is tuned to be largest around $4.0\,\mathrm{GeV}/c^2$. In the non-resonant (NR) process, the angular momentum $(L_{K^+X}, L_{D_s^-D^{*0}})$ denotes the angular momentum between K^+ and $X_{D_s^-D^{*0}}$, and D_s^- and D^{*0} in the $e^+e^-(X_{D_s^-D^{*0}})$ rest frame, respectively. Individual contributions are scaled according to the observed yields in the control samples.

III. SYSTEMATICS UNCERTAINTIES

Sources of systematic uncertainties on the measurement of the $Z_{cs}(3985)^-$ resonance parameters and the cross section are studied, in which the main sources include the mass scaling, detector resolution, the signal model, background models and the input cross-section line shape for $\sigma^B(e^+e^- \to K^+ Z_{cs}(3985)^-)$.

We select a control sample of $e^+e^- \to D_{s1}(2536)^+ D_s^{*-} \to K^+ D^{*0} D_s^{*-}$ at $\sqrt{s} = 4.681$ GeV by detecting $K^+ D^{*0}$ with $D^{*0} \to \pi^0 D^0$, $D^0 \to K^-\pi^+$, $K^-\pi^+\pi^0$ as well as $K^-\pi^+\pi^+\pi^-$ with a missing D_s^{*-} in the final state to study the mass scaling of the recoil mass of the low-momentum bachelor K^+. We fit the D_s^{*-} peak in the spectra of the recoil mass of K^+D^{*0}, where the D_s^{*-} signal is modeled with a MC-determined signal shape convolved with a Gaussian function to represent a potential difference between data and MC simulation. The fitted Gaussian parameters are determined to be $\mu = -0.2 \pm 0.5\,\mathrm{MeV}/c^2$ and $\sigma_{\mathrm{upper}} < 1.43\,\mathrm{MeV}$ (68% C.L.), which are used to determine the systematic effects due to mass scaling and detection resolution. After incorporating the evaluated detection resolution difference up to the upper uncertainty, we find the maximum change on the result of the fitted width to be 1.0 MeV.

In this work the two Z_{cs} signal processes are difficult to distinguish due to the partial-reconstruction method and the limited sample size. Hence, without any a priori knowledge, we vary the BF ratio f in the range from 0.2 to 0.8, corresponding to the standard deviation of a uniform distribution from 0 to 1. We find the resulting changes on the mass and width to be $0.2\,\mathrm{MeV}/c^2$ and 1.0 MeV, respectively. In the nominal fit, we assume that the spin-parity of the $Z_{cs}(3985)^-$ is 1^+ and that the relative momentum between K^+ and $Z_{cs}(3985)^-$ in the rest frame of the e^+e^- system and the relative momentum between $D_s^-(D_s^{*-})$ and $D^{*0}(D^0)$ in $Z_{cs}(3985)^-$ system are both in an S-wave state, denoted as $1^+(S,\, S)$. This hypothesis can only be verified by an amplitude analysis of the signal final states, which is not feasible with the current statistics. Therefore, as systematic variations, we test the assumptions of spin-parity and angular momentum with $1^+(D,\, S)$, $0^-(P,\, P)$, $1^-(P,\, P)$ and $2^-(P,\, P)$ configurations. These tests give maximum changes of $1.0\,\mathrm{MeV}/c^2$ in the mass and 2.6 MeV in the width. The systematic uncertainty related to the combinatorial background is estimated by varying both the sideband yield within its uncertainties and the background parametrization; the quadrature sums of each largest difference from the nominal fit are $0.5\,\mathrm{MeV}/c^2$ and 0.5 MeV for the mass and width, respectively, which are taken as the systematic uncertainties. The efficiency curves adopted in the resonance fit are varied within the uncertainties of their parametrizations, and the differences of $0.1\,\mathrm{MeV}/c^2$ in mass and 0.2 MeV in width to the nominal fit are taken as the related systematic uncertainty.

Any potential effects of the known $D_{(s)}^{**}$ states (as listed in Table I) on the measurements are evaluated. We vary the size of the D_s^{**+} and $\bar{D}_3^*(2750)^0$ background components within their uncertainties in the fit and take the variations as systematic uncertainties. For the known $\bar{D}^{**0}$ states, which have $RM(K^+)$ distributions similar to that of the NR signal, the fit is repeated with each state as an additional component with its shape taken from MC simulation and the yield as a free parameter. To further check the $\bar{D}_1^*(2600)^0$ component, we remove the NR component from the simultaneous fit. The ratio $\mathcal{B}(\bar{D}_1^*(2600)^0 \to D_s^- K^+)/\mathcal{B}(\bar{D}_1^*(2600)^0 \to D^-\pi^+)$ then increases from 0.00 ± 0.02 to 0.12 ± 0.02. We evaluate the quadrature sum of the mass and width differences between each of the results from these alternative fits with respect to the nominal fit and assign the quadrature sums as related systematic uncertainties of $1.0\,\mathrm{MeV}/c^2$ for the mass and 3.4 MeV for the width. We vary the input Born cross section $\sigma^B(e^+e^- \to K^+ Z_{cs}(3985)^-)$ within the uncertainties and repeat the signal extraction, which gives a maximum change of $0.6\,\mathrm{MeV}/c^2$ for the mass and 1.7 MeV for the width.

Other systematic effects mostly influence the measurement of the cross section. Average uncertainties associated with the tracking, PID and K_S^0 reconstruction efficiencies are estimated to be 3.6%, 3.6% and 0.4%, respectively. The efficiency of the $RM(K^+D_s^-)$ requirement is re-estimated by changing the MC-simulated resolution according to the observed difference with respect to data and the resulting change is taken as the systematic uncertainty on the cross section. The integrated-luminosity uncertainty, measured with large-angle Bhabha events, is estimated to be 1%. The uncertainties on the quoted BFs for the involved decays [1] are included as part of the systematic uncertainty.

Table II summarizes the systematic uncertainties on the cross sections at $\sqrt{s}$=4.628, 4.641, 4.661, 4.681 and 4.698 GeV.

TABLE II. Summary of systematic uncertainties on the cross sections at different energy points. The total systematic uncertainty corresponds to a quadrature sum of all individual items.

Source	$\sigma_{4.628}\mathcal{B}(\%)$	$\sigma_{4.641}\mathcal{B}(\%)$	$\sigma_{4.661}\mathcal{B}(\%)$	$\sigma_{4.681}\mathcal{B}(\%)$	$\sigma_{4.698}\mathcal{B}(\%)$
Tracking	3.6	3.6	3.6	3.6	3.6
Particle ID	3.6	3.6	3.6	3.6	3.6
K_S^0	0.4	0.4	0.4	0.4	0.4
$RM(K^+D_s^-)$	4.0	0.3	0.4	0.6	0.2
Resolution	0.2	1.0	1.9	1.1	0.8
f factor	7.8	7.7	6.7	6.4	5.9
Signal model	20.5	14.4	16.6	21.9	11.2
Backgrounds	54.8	5.9	12.0	3.1	7.8
Efficiencies	0.2	0.2	0.2	0.5	0.1
$D_{(s)}^{**}$ states	47.1	82.2	35.3	15.7	35.3
$\sigma^B(K^+Z_{cs}(3985)^-)$	11.9	5.7	22.1	13.4	32.1
Luminosity	1.0	1.0	1.0	1.0	1.0
Input BFs	2.7	2.7	2.7	2.7	2.7
total	76.8	84.5	47.3	31.5	50.3

IV. FIT RESULTS BASED ON THREE SUBSETS OF DATA SET AT $\sqrt{s} = 4.681$ GeV

To avoid potential bias, the analysis strategy is firstly implemented and validated using the first one-third of data set at $\sqrt{s} = 4.681$ GeV, where the fit result is shown in Fig. 7(left) and given in Table III. Afterward, we split the two-thirds of data into two parts for consistency check by implementing the same fit procedures, the results of which are depicted in Fig. 7(middle) and (right). The corresponding numerical results are listed in Table III. The fitted resonance parameters between the 1st and 2nd one-third of data set are consistent within statistical uncertainty, while the comparison between the 1st and 3rd one-third of data set shows that the fitted masses and widths are in agreement within 1.5σ and 1.0σ, respectively. Overall, the three sets of fit results are compatible and we can assume they are due to the same source. Hence, the three parts of data at $\sqrt{s} = 4.681$ GeV are combined to obtain the nominal fit results listed in Table III.

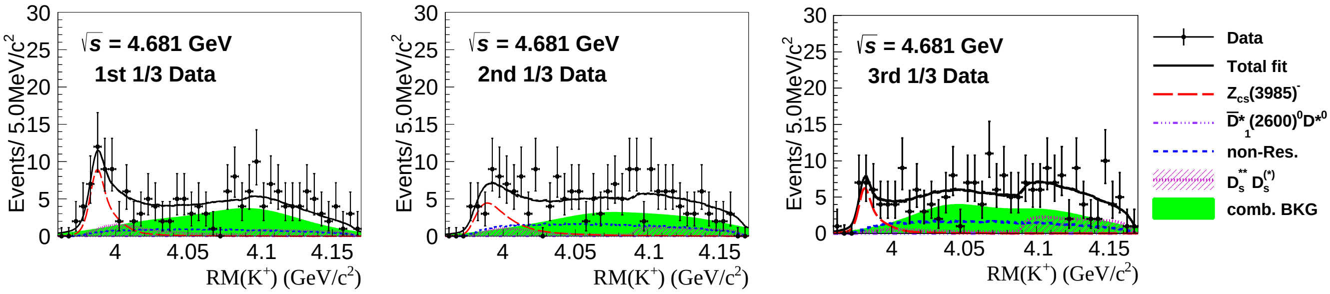

FIG. 7. Fit to the K^+ recoil mass spectra in the first (left), second (middle) and third (right) one-third of data set at $\sqrt{s} = 4.681$ GeV.

TABLE III. Fit results of the $Z_{cs}(3985)^-$ resonance parameters and cross sections based on the first, second and third one-third of data set at $\sqrt{s} = 4.681$ GeV.

Data set	Mass (MeV/c^2)	Width (MeV)	$\sigma_{4.681} \cdot \mathcal{B}$(pb)	Statistical Significance
1st one-third	$3987.0^{+2.1}_{-2.4}$	$6.9^{+6.1}_{-4.1}$	$5.1^{+1.4}_{-1.2}$	4.9σ
2nd one-third	$3990.2^{+5.6}_{-5.5}$	$24.2^{+31.0}_{-12.4}$	$5.0^{+2.3}_{-1.8}$	2.9σ
3rd one-third	$3980.9^{+2.0}_{-2.2}$	$4.7^{+9.9}_{-4.7}$	$2.8^{+1.2}_{-1.0}$	3.9σ
nominal	$3985.2^{+2.1}_{-2.0}$	$13.8^{+8.1}_{-5.2}$	$4.4^{+0.9}_{-0.8}$	6.3σ

V. CALCULATION OF THE POLE MASS AND WIDTH

The pole position $m_{\rm pole}(Z_{cs}(3985)^-) - i\frac{\Gamma_{\rm pole}(Z_{cs}(3985)^-)}{2}$ is determined by solving the equation

$$\begin{cases} M^2 - m_0^2 + im_0(f\Gamma_1(M) + (1-f)\Gamma_2(M)) = 0, \\ \Gamma_1(M) = \Gamma_0 \cdot \dfrac{p_1}{p_1^*} \cdot \dfrac{m_0}{M}, \\ \Gamma_2(M) = \Gamma_0 \cdot \dfrac{p_2}{p_2^*} \cdot \dfrac{m_0}{M}, \end{cases} \tag{1}$$

where the input values of m_0 and Γ_0 are taken from the simultaneous fit. The resonance mass is above the mass thresholds of the two coupled channels and the pole position is taken from Riemann sheet III defined in Ref. [2]. To properly account for their correlations, a Monte-Carlo method is adopted, in which pseudo data of m_0 and Γ_0 are generated according to the correlation matrix to calculate the pole position.

[1] P. A. Zyla *et al.* (Particle Data Group), Prog. Theor. Exp. Phys. **2020**, 083C01 (2020).
[2] A. M. Badalian, L. P. Kok, M. I. Polikarpov and Y. A. Simonov, Phys. Rept. **82**, 31 (1982).